JGR Oceans

RESEARCH ARTICLE
10.1029/2020JC016217

Decadal Strengthening of Interior Flow of North Atlantic Deep Water Observed by GRACE Satellites

Jannes Koelling[1,2], **Uwe Send**[1], **and Matthias Lankhorst**[1]

[1]Scripps Institution of Oceanography, University of California San Diego, La Jolla, CA, USA, [2]Ocean Frontier Institute, Department of Oceanography, Dalhousie University, Halifax, Nova Scotia, Canada

Key Points:
- GRACE ocean mass trends are validated using mooring and altimetry data
- Changes reveal decadal variability in the deep circulation of the North Atlantic ocean
- Flow of North Atlantic Deep Water in the interior strengthened compared to the boundary circulation

Supporting Information:
- Supporting Information S1

Correspondence to:
J. Koelling,
j.koelling@dal.ca

Citation:
Koelling, J., Send, U., & Lankhorst, M. (2020). Decadal strengthening of interior flow of North Atlantic Deep Water observed by GRACE satellites. *Journal of Geophysical Research: Oceans*, *125*, e2020JC016217. https://doi.org/10.1029/2020JC016217

Received 6 MAR 2020
Accepted 17 OCT 2020
Accepted article online 22 OCT 2020

Abstract The Gravity Recovery and Climate Experiment (GRACE) satellite mission provides information on changes to the Earth's gravity field, including ocean mass. Long-term trends in GRACE data are often considered unreliable due to uncertainties in the corrections made to calculate ocean mass from the raw measurements. Here, we use an independent estimate of ocean mass from satellite altimetry and in situ density data from five mooring sites and repeat hydrography to validate trends in GRACE over the North Atlantic, finding substantial agreement between the methods. The root-mean-square difference between ocean mass changes calculated with this method from the mooring data and those measured by GRACE is 3.5 mm per decade, much lower than the mean signal of 15.6 ± 1.8 mm per decade for GRACE and 17.8 ± 5.2 mm per decade for the altimetry-mooring estimate. The GRACE ocean mass data are then used to study the change in the deep circulation of the North Atlantic between the 1 April 2002 to 31 March 2009 and 1 April 2010 to 31 March 2017 periods, revealing a large-scale anticyclonic circulation anomaly off the North American coast. The change is associated with an increase of 13.9 ± 3.3 Sv ($1\ \text{Sv} = 10^6\ \text{m}^3\ \text{s}^{-1}$) of southward North Atlantic Deep Water flow in the interior between 30°N and 40°N, largely balanced by a northward anomaly of 10.7 ± 3.3 Sv for the boundary circulation. This implies an increased importance of interior pathways compared to the Deep Western Boundary Current for the spreading of North Atlantic Deep Water, which constitutes the lower limb of the Atlantic Meridional Overturning Circulation.

Plain Language Summary The Gravity Recovery and Climate Experiment (GRACE) satellites measure the Earth's gravity field, which can be used to study ocean currents. In this study, we validate long-term trends in the data using independent ocean measurements to confirm that they reflect real changes in the ocean. In the Atlantic Ocean, North Atlantic Deep Water flows southward from its formation region near Greenland, spreading throughout the ocean basin. The flow of North Atlantic Deep Water is a crucial part of Earth's climate system, making it an important process to understand. Most of the water spreads southward in the so-called Deep Western Boundary Current along the continental shelves of North America, but there is also a significant flow further offshore in the interior of the basin. We use the GRACE data to measure changes to these two pathways between the 2002–2009 and 2010–2017 periods. The results show that southward flow in the interior has strengthened during this time, with opposite changes near the continent. This marks a significant change to how this water spreads from the formation region.

1. Introduction

The Gravity Recovery and Climate Experiment, or GRACE, satellite mission was launched in 2002 (Tapley et al., 2004), and collected an approximately 15-year-long record of variability in the Earth's gravity field before it was decommissioned in late 2017. The follow-on mission, GRACE-FO, was launched in May 2018 (Landerer et al., 2020). The GRACE setup consists of twin satellites orbiting the Earth in sequence and measuring the change in distance between one another using radar. Changes in the Earth's gravity field accelerate or decelerate each of the satellites as they pass above them, and the resulting change in the distance between the satellites is used to infer gravity anomalies. Gravity changes over the ocean provide information on ocean mass variability, which is used for studies of the global sea level budget (Chambers et al., 2017; Leuliette & Miller, 2009) and deep ocean circulation (Landerer et al., 2015; Mazloff & Boening, 2016). Early GRACE products suffered from spurious "leakage" of the much larger terrestrial signal into the ocean, particularly near the coasts (Guo et al., 2010). Several gridded products developed since

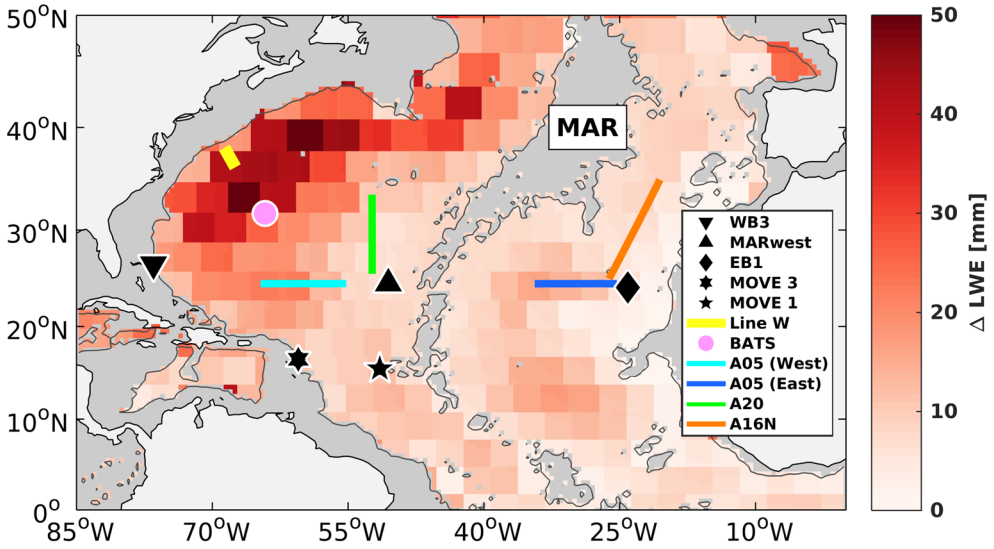

Figure 1. Ocean mass change in the GRACE JPL RL05.1 M product, calculated as the mean from 1 April 2010 to 31 March 2017 minus the mean from 1 April 2002 to 31 March 2009. Data are only shown at grid points with depths exceeding 3500 m, and expressed as liquid water equivalent (LWE). Black symbols denote mooring sites, and other symbols/lines show repeat hydrography stations and sections used in this study. Shading shows the 3,500-m isobath, and MAR refers to the Mid-Atlantic Ridge.

then address this issue by separating the global grid into spherical cap mass concentrations, or mascons, which better differentiate between land and ocean. Nonetheless, uncertainties remain as large signals unrelated to oceanic variability, such as glacial isostatic adjustment or the Earth's pole tide, need to be corrected to obtain the final GRACE solution, and errors in estimating these quantities can propagate into the gridded GRACE data. These geophysical processes occur on time scales far exceeding the length of the GRACE record, such that they would manifest themselves as trends in the ocean mass data (Watkins et al., 2015). As a result, linear trends are often removed from GRACE data before using them in transport calculations (Landerer et al., 2015; Worthington et al., 2019). However, since changes in ocean mass are related to geostrophic flow through their effect on bottom pressure, the signal on these time scales is of great interest for studies of the deep circulation. This is true particularly in the Atlantic Ocean, where they are associated with variability in the lower branch of the Atlantic Meridional Overturning Circulation (AMOC), which plays an important role in the Earth's climate (Srokosz & Bryden, 2015). Decadal variability and long-term trends in AMOC strength have been shown to exist in both observations and climate models (Danabasoglu, 2008; Muir & Fedorov, 2017; Send et al., 2011; Smeed et al., 2014), and the much better spatial coverage of GRACE compared to traditional measurements in the deep ocean could provide new insights into variability of the deep circulation. In the North Atlantic ocean, the decadal signal in GRACE appears to exhibit large-scale patterns of ocean mass increase which are intensified in the interior western basin (Figure 1), resembling patterns associated with the distribution of North Atlantic Deep Water (NADW) (Rhein et al., 2015). This study is motivated by the question of whether or not these changes reflect real oceanic variability.

Although continuous time series of in situ ocean bottom pressure (OBP) for comparison to GRACE do exist, bottom pressure recorders suffer from a drift that is difficult to separate from real variability on time scales longer than a few years (Watts & Kontoyiannis, 1990), rendering them unsuitable for validating trends in GRACE. An alternative method of inferring variability in ocean mass is to calculate it as the difference between sea level anomalies and changes in steric height, the latter being caused by the expansion or contraction of the water column due to density changes. An analysis of hydrographic data by Purkey et al. (2014) showed that global ocean mass trends calculated with this method agreed well with an earlier release of GRACE data, and regional trends averaged over entire ocean basins were generally consistent with GRACE, too. To date, this method has not been employed on smaller spatial scales due to the temporal and spatial sparsity of full water column ocean density data, which results in small-scale noise being aliased into the larger-scale signal of interest. However, a model simulation by Williams et al. (2015) showed that, using thorough calibration procedures for mooring data, sufficient accuracy can be achieved to detect decadal trends

Table 1
Access Information for Data Used in This Study

Site	Website	Data version or access date
RAPID WB3, MARwest	http://rapid.ac.uk	05/2019
RAPID EB1	http://bodc.ac.uk	10/2018
MOVE 3, MOVE 1	ftp://data.ndbc.noaa.gov/data/oceansites/DATA/	04/2018
A05, A20, A16N	http://cchdo.ucsd.edu	02/2017
BATS	http://cchdo.ucsd.edu	11/2018
Line W	http://scienceweb.whoi.edu/linew	05/2017
GRACE	http://grace.jpl.nasa.gov	JPL RL05.1M
Altimetry	http://aviso.altimetry.fr *(now available at marine.copernicus.eu)*	dt_global_twosat_madt

from moorings and satellite altimetry. Carefully calibrated mooring arrays have been deployed as part of the MOVE project at 16°N since 2000 (Send et al., 2011), and the RAPID project at 26.5°N since 2004 (McCarthy et al., 2015). Here, we use data from these moorings, along with hydrographic time series and transects, to validate decadal trends in GRACE (Figure 1), and subsequently use these GRACE data to investigate the corresponding changes to the deep circulation of the Atlantic Ocean.

2. Methods and Data

2.1. Data

Both MOVE and RAPID moored conductivity-temperature-depth (CTD) data are calibrated before and after each deployment by attaching each sensor to a ship-based rosette with CTD sensor and comparing measurements during a number of subsurface stops to data from the rosette CTD, which in turn is calibrated against bottle samples. The resulting accuracy of the practical salinity, temperature, and pressure measurements is 0.002, 0.001°C, and 2 dbar relative to the rosette CTD (Kanzow et al., 2006). For the MOVE moorings, anomalies of temperature (T) and salinity (S) from climatology are interpolated vertically between sensors to produce a data set on a consistent vertical grid. MOVE 1 was deployed in a different configuration between 2007 and 2011, with no instruments in the upper 1,000 m of the water column, resulting in a data gap of approximately 4 years in the steric height data used here. Data from the RAPID *EB1* mooring are processed the same way, with data from each instrument obtained from https://www.bodc.ac.uk/ website. For the RAPID *WB3* and *MARwest* moorings, temperature and salinity data are taken from the pressure-gridded fields available on the project website, http://www.rapid.ac.uk/ (Smeed et al., 2019). These extend from the seafloor to about 150 m below the sea surface throughout the deployments. The procedure for interpolation between instruments is similar to that used at MOVE and is described in more detail by McCarthy et al. (2015).

For all mooring data, the steric height measurements used in this study are extrapolated above the shallowest measurement by a linear fit to steric height anomalies based on the method described by McCarthy et al. (2015). The data used for the linear fit are taken from the 75 m below the uppermost mooring instrument at each site. Shipboard data from the Bermuda Atlantic Time Series (BATS), Line W, and hydrographic transects A05, A20, and 16N are also used. The sources for all data used in this study are listed in Table 1, and the times and locations of measurements used are given in Table 2.

For altimetry data, the daily gridded two-satellite product is used, which uses one satellite as a reference in order to obtain a stable signal on climate-relevant time scales. The altimetry data are linearly interpolated to the location of the respective density measurements, and averaged over 10 days when used with shipboard data. GRACE data come from the JPL RL05.1 M product, the development of which was motivated in part by a desire to improve the representation of gravity anomalies over the ocean (Watkins et al., 2015). The method involves separating the Earth into 4,551 equal-area mass concentration cells, called mascons, with an area equivalent to 3° × 3° at the equator, and integrating the gravitational potential over the surface of each mascon. Thus, while the grid spacing of the data product is 0.5° × 0.5°, the effective resolution is about 3° × 3°. The usage of the mascons eliminates much of the spurious north-south "stripe" signal found in earlier spherical harmonic solutions (Save et al., 2016; Watkins et al., 2015), and improves the separation between gravity signals in the ocean and on land. For details on the mascon method, and its advantages over

Table 2
Components of the Sea Level Budget (in Millimeters per Decade)

Mooring site	Time period	ΔSL_{alt}	ΔSL_{steric}	ΔSL_{mass}(A&S)	ΔSL_{mass}(G)	
RAPID WB3	1 April 2004 to 31 March 2017	98.0 ± 6.6	65.7 ± 7.4	32.3 ± 10.0	28.9 ± 2.2	
RAPID MARwest	1 April 2004 to 31 March 2017	37.5 ± 9.5	24.9 ± 7.4	12.6 ± 12.0	12.2 ± 1.6	
RAPID EB1	1 April 2005 to 31 March 2017	41.0 ± 9.6	25.8 ± 8.1	15.2 ± 12.6	8.4 ± 1.9	
MOVE 3	1 April 2002 to 31 December 2014	0.2 ± 7.8	−13.0 ± 8.7	13.2 ± 11.7	13.9 ± 2.2	
MOVE 1	1 April 2002 to 31 March 2015[a]	24.6 ± 8.3	8.9 ± 9.1	15.7 ± 12.4	14.7 ± 1.2	
Mean				17.8 ± 5.2	15.6 ± 1.8	RMSD:3.5
Transect/station	Time period	Lat/lon range or station		ΔSL_{mass}(A&S)	ΔSL_{mass}(G)	
A05	April 2004, January 2015	65–55°W, 24.5°N		21.6 ± 17.1	21.8 ± 5.9	
A05	April 2004, January 2015	35–25°W, 24.5°N		22.9 ± 19.2	14.7 ± 5.9	
A20	October 2003, May 2012	52°W, 25–35°N		10.9 ± 18.7	9.2 ± 5.9	
A16N	July 2003, August 2013	26.2–20.6°W, 25–35°N		9.2 ± 15.7	7.9 ± 5.9	
Line W	September 2003 to June 2013	68.7°W, 38.1°N to 67.5°W, 36.2°N		48.9 ± 11.6	57.4 ± 10.3	
BATS	1 January 2002 to 31 December 2016	64.4–63.9°W, 31.4–31.9°N		22.6 ± 6.9	31.5 ± 1.6	
Mean				22.7 ± 5.8	23.8 ± 2.4	RMSD:6.1

Note. Uncertainties represent the instrumental error (section 2.4). ΔSL_{alt}: Sea surface height change from satellite altimetry. ΔSL_{steric}: Steric height change from in situ density data; ΔSL_{mass}(A&S): ocean mass change calculated as the difference between ΔSL_{alt} and ΔSL_{steric}; ΔSL_{mass}(G): ocean mass change from GRACE over the same time period.
[a]No data for MOVE 1 between August 2006 and December 2010.

previous GRACE products, the reader is referred to Watkins et al. (2015) and Wiese et al. (2016). The GRACE data are corrected for errors in the pole tide model following Wahr et al. (2015). Changes in atmospheric mass over the ocean are not corrected for in this study, but the effect of this correction on the trends would be less than 1 mm per decade, much smaller than the signal seen in Figure 1. Data used for each site are taken from the nearest grid point. BATS lies on the boundary between two GRACE mascons, one encompassing much of the shallow ocean around Bermuda, and one situated largely in the deep ocean, with the latter chosen for the analysis here.

2.2. Sea Level Budget

Sea level anomaly relative to a reference time measured by satellite altimetry, SL'_{alt}, can be expressed as the sum of two components, one due to expansion or contraction of the water column as a result of density changes, SL'_{steric}, and one due to addition or subtraction of mass, SL'_{mass}. In this study, we use mooring- and hydrography-based measurements of T and S profiles to calculate SL'_{steric} for the full water column and combine them with SL'_{alt} to obtain an estimate of SL'_{mass}:

$$SL'_{mass}(t) = SL'_{alt}(t) - SL'_{steric}(t) \quad (1)$$

where t is time. Steric height is computed as

$$SL_{steric} = g^{-1} \int_{p_{ref}}^{0} \delta dp \quad (2)$$

where g is the gravitational constant, δ is the specific volume anomaly relative to seawater at a salinity of 35 and temperature of 0°C (Talley et al., 2012), and the integration limits are the sea surface and a reference pressure p_{ref}. Studies of global sea level rise have compared total sea level anomalies, SL'_{alt}, calculated from SL'_{steric} from Argo floats, and SL'_{mass} from GRACE, to sea level records from tide gauges or altimetry in an attempt to close the global sea level budget (e.g., Chambers et al., 2017; Leuliette & Miller, 2009). However, Argo floats only sample the upper 2,000 m of the ocean, so that variability below cannot be resolved from these measurements alone. Here, SL'_{steric} is computed by integrating over most of the water column, with the deepest measurement available throughout the record, typically between 4,000 and 5,000 m, chosen as the reference depth at each site.

We calculate the ocean mass trend in millimeters per decade as the difference between the average of SL'_{mass} (in mm) over two multiyear periods, T_1 and T_2, scaled by the time difference between the central time in each period, ΔT, in years:

$$\Delta SL_{\text{mass}} = \left(\overline{SL'_{\text{mass}}}^{T_2} - \overline{SL'_{\text{mass}}}^{T_1}\right) \frac{10}{\Delta T} \tag{3}$$

where overbars denote the time average. Using the above equation, a trend is calculated from the GRACE ocean mass data, ΔSL_{mass}(G). Ocean mass is also calculated from altimetry (A) and steric height from density data (S) using Equation 1 and used in Equation 3 to obtain a second estimate of the trend. We refer to this as the altimetry-steric height estimate of ocean mass, ΔSL_{mass}(A&S). The two are compared in section 3.1 to evaluate the veracity of trends in the GRACE data.

For moorings and the regularly sampled BATS hydrography data, the averages are taken over the first and second half of the record, calculated for an integer number of years. For example, for the 13-year RAPID record, changes are calculated as the difference between the 1 April 2004 to 31 March 2010 and 1 April 2011 to 31 March 2017 periods. Line W was only occupied once or twice per year over a 10-year period. To achieve a robust estimate here, the trends between the first and second half of the record are averaged over eight stations, and the mean of these stations is used in section 3.1. The station numbers used are # 9014-9021, and their longitude/latitude range is given in Table 2. For other hydrographic transects, data come from only two occupations, and therefore short-term and small-scale variability can alias the long-term difference sought here. To mitigate this, the hydrography data are averaged over a relatively broad longitude or latitude range to reduce noise associated with variability on small spatial scales. The averaging for each transect includes about 10 to 20 stations, and the ranges are given in Table 2. For consistency, trends from GRACE are averaged over the same regions. In addition, $\overline{SL'_{\text{mass}}}^{T_n}$ is calculated as

$$\overline{SL'_{\text{mass}}}^{T_n}(\text{A\&S}) = SL'_{\text{mass}}(\text{A\&S})(t_n) - \left(SL_{\text{mass}}(\text{G})(t_n) - \overline{SL'_{\text{mass}}}^{T_n}(\text{G})\right) \tag{4}$$

where t_n denotes the time of the CTD occupation (see Table 2), and T_n is a multiyear period as in Equation 3. $SL_{\text{mass}}(\text{G})(t_n)$ is averaged over 3 months centered on t_n, and $\overline{SL'_{\text{mass}}}^{T_n}(\text{G})$ is calculated for 1 April 2002 to 31 March 2009 and 1 April 2010 to 31 March 2017, for T_1 and T_2, respectively. This removes some of the higher-frequency variability associated with seasonal or interannual variability in $SL'_{\text{mass}}(\text{A\&S})(t_n)$ based on GRACE data, so that the resulting estimate ΔSL_{mass}(A&S) is more representative of the long-term trend. The method to calculate trends from single occupations of hydrography lines from Equation 4 is shown schematically in Figure S1 in the supporting information.

2.3. Geostrophic Transport

The change in horizontally averaged geostrophic flow between any two points at the same depth, z_1 as a function of pressure p, is given by

$$u'(z_1) = -\frac{1}{f\rho_0}\frac{\Delta p'(z_1)}{\Delta y}, v'(z_1) = \frac{1}{f\rho_0}\frac{\Delta p'(z_1)}{\Delta x} \tag{5}$$

with ρ_0 and f being a typical seawater density and the Coriolis parameter, respectively, and primes denoting fluctuations relative to the time mean. Ocean bottom pressure can be inferred from GRACE ocean mass, which can thus be used to calculate the geostrophic flow at this depth. In this study, the change in the OBP gradient between two adjacent points with different bottom depths is taken to represent the change in the flow at the shallower of the two depths. To verify that this is a valid assumption, we analyzed decadal changes in velocity shear from the World Ocean Atlas product (Levitus et al., 2013). The decadal change in the sheared component of the deep ocean circulation between neighboring grid points in the study domain is typically on the order of 100 $\text{m}^2\,\text{s}^{-1}$, much smaller than the change from the GRACE data seen in Figure 5.

A vertically resolved profile of velocity changes can be obtained by using the deepest common level between two points as the reference level, and calculating velocity shear relative to this level from the horizontal density gradient. Integrating this profile in depth yields the change in transport, which can be separated into a barotropic component T'_{BT} calculated from OBP changes, and a baroclinic component, T'_{BC}, calculated from the velocity shear.

2.4. Error Sources

2.4.1. Instrumental Error

The accuracy of individual altimetry measurements of sea surface height is about 2.5 cm for modern altimeters (Chelton et al., 2001), so the error for SSH averaged over a certain time period or region is given by

$$\sigma_{\text{SSH}} = \frac{2.5\text{cm}}{\sqrt{DOF_{\text{SSH}}}} \tag{6}$$

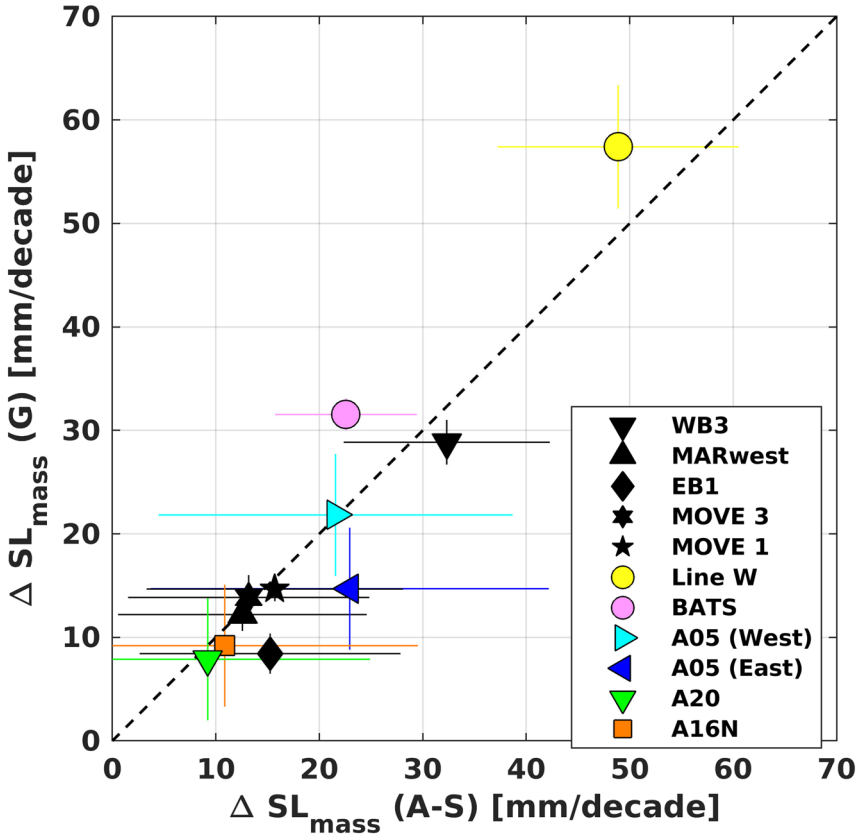

Figure 2. ΔSL_{mass}(G) from GRACE compared to ΔSL_{mass}(A&S) calculated as the difference between ΔSL_{alt} from altimetry and $\Delta SL_{\text{steric}}$ from moorings (black symbols) or hydrography data (other colors). Error bars show instrumental error (section 2.4). Symbols and colors correspond to those in Figure 1. The black dashed line shows a 1:1 slope.

with DOF_{SSH} representing the degrees of freedom of the average. To derive the degrees of freedom, an autocorrelation time scale τ is calculated following Leith (1973), and the degrees of freedom are calculated as $DOF_{\text{SSH}} = L/\tau$, where L is the length of the time series for each averaging period. For CTD data from hydrographic transects used in Figure 2, we assume that SSH data at each station are independent, such that DOF_{SSH} is equal to the number of stations used in the averaging.

For mooring-based steric height estimates, the error comes principally from two sources: the calibration error of each instrument relative to the reference CTD in the calibration procedures described in Kanzow et al. (2006), σ_{inst}, and the accuracy of the reference CTD itself in measuring temperature, salinity, and pressure, σ_{CTD}. For σ_{inst}, we use a value of 4 mm, which was determined by Williams et al. (2015) to be the uncertainty in steric height due to uncorrelated calibration errors for individual instruments. The CTD error is calculated by considering separately the contributions of the measurement accuracy of 0.002°C and 0.002°C on salinity and temperature (IOCCP-ICPO, 2010), and an error of 0.0015% of full scale, or about 1.02 dbar, for a typical pressure sensor (Houston & Paros, 1998). The combined error σ_{CTD} amounts to about 8.2 mm for a typical depth of 5,000 m, and scales approximately linearly with depth. The error for the steric height in each of the two time periods T is then given by

$$\sigma_{\text{steric}}(\text{T}) = \sqrt{\frac{\sigma_{\text{inst}}^2 + \sigma_{\text{CTD}}^2}{DOF_{\text{steric}}(\text{T})}} \tag{7}$$

Measurements from the same mooring deployment cruise cannot be considered independent as they are calibrated against the same CTD data, such that the degrees of freedom $DOF_{\text{steric}}(T)$ for each time period T are equal to the number of mooring deployments during this time. For estimates from single CTD sections, $\sigma_{\text{inst}} = 0$, but the overall error is larger because they come from only one cruise, so that $DOF_{\text{steric}}(T) = 1$.

For moorings, there is also an error associated with the discrete sampling in the vertical (Kanzow et al., 2006). This is typically about 1 cm for instantaneous steric height measurements (Williams et al., 2015), but unlike σ_{inst} and σ_{CTD}, the error is not constant for each deployment. The degrees of freedom are therefore given by the autocorrelation time scale of the measurement (Leith, 1973), with resulting errors in the trend on the order of 1 mm per decade, which is negligible compared to σ_{inst} and σ_{CTD}.

Assuming errors are uncorrelated, the total error for the altimetry-steric height estimate of ocean mass change, ΔSL_{mass}(A&S), is then

$$\sigma_{\Delta SL_{\text{mass}}(\text{A\&S})} = \sqrt{\sigma^2_{\text{steric}}(T_1) + \sigma^2_{\text{steric}}(T_2) + \sigma^2_{\text{SSH}}(T_1) + \sigma^2_{\text{SSH}}(T_2)} \tag{8}$$

The uncertainty in GRACE is calculated from a measurement error of 1 cm (Landerer et al., 2015; Watkins et al., 2015), and the degrees of freedom calculated from the length of the time series and the autocorrelation time scale. Error bars in Figure 2 and uncertainties in Table 2 reflect the instrumental error discussed in this section.

2.4.2. Other Errors

In addition to the measurement error, biases in regional trends from satellite altimetry can be on the order of 2–3 mm year^{-1} due mostly to orbit errors (Ablain et al., 2015), which is of comparable magnitude to the ocean mass trends shown in Figure 1. For GRACE, uncertainties in the removal of low-frequency signals that are not related to oceanic variability are also of the same order as the signal of interest (Landerer et al., 2015), and the large averaging area of the GRACE mascons smooths out some of the signal compared to the point measurements from moorings and higher-resolution data from altimetry. The magnitude of all of these errors will depend on the location, making them difficult to quantify, so they are not shown as part of the uncertainty in Figure 2 and Table 2. We note that the bias from corrections to altimetry or GRACE alone could feasibly be responsible for the entire trend at most sites. However, the good agreement between the two methods of calculating SL_{mass} and the spatial patterns in the trend (see below) suggests that this is not the case.

3. Ocean Mass Changes

Spatially variable decadal ocean mass changes are evident in the GRACE data in Figure 1, but previous studies have typically assumed the trends to be caused by uncertainties in the GRACE correction (Landerer et al., 2015). In this section, we evaluate whether observed trends reflect real ocean mass changes, or whether they are spurious trends introduced by errors in the data processing. We also compare spatial patterns of the trend to water mass properties and investigate the contribution of different parts of the water column to steric height changes.

3.1. Validating Decadal Trends in GRACE

To validate the decadal ocean mass change seen in Figure 1, ΔSL_{mass}(A&S) is calculated as the difference between ΔSL_{alt} from altimetry and $\Delta SL_{\text{steric}}$ from moorings (Equations 1 and 3). This estimate of the ocean mass trend is plotted against the trend over the same time period from the GRACE JPL RL05.1 M product, ΔSL_{mass}(G), with black symbols in Figure 2. Both estimates are listed for all moorings in Table 2. SL'_{mass}(A&S) increased at all sites, with values ranging from 12.6 ± 12.0 to 32.3 ± 10.0 mm per decade. The range of GRACE ocean mass changes calculated over the same periods is 8.4 ± 1.9 to 28.9 ± 2.2 mm per decade. The mean increase in ocean mass at all mooring sites is comparable for the altimetry-mooring and GRACE estimates at 17.8 ± 5.2 mm per decade for ΔSL_{mass}(A&S) and 15.6 ± 1.8 mm per decade for ΔSL_{mass}(G). The root-mean-square difference, or RMSD, between ocean mass changes for the five moorings calculated from Equation 1 and those measured by GRACE at the respective sites is 3.5 mm per decade. The RMSD is less than a quarter of the mean trend, and lower than the smallest observed change of 8.4 ± 1.9 mm per decade, demonstrating that the two methods yield consistent results. The agreement is also much better than the accuracies typically given for trends in both the altimetry and GRACE ocean mass measurements. The mismatch is only about 18% of the 2- to 3-mm year^{-1} regional error for altimetry (Ablain et al., 2015), and 35% of the 1-mm year^{-1} uncertainty for GRACE (Quinn & Ponte, 2010), suggesting that errors in the trend may be smaller than previously thought.

Repeating the same analysis with different data products of GRACE yields larger RMS differences with ΔSL_{mass}(A&S) of about 14 mm per decade for the earlier JPL RL05.1 (nonmascon) solution and the CSR

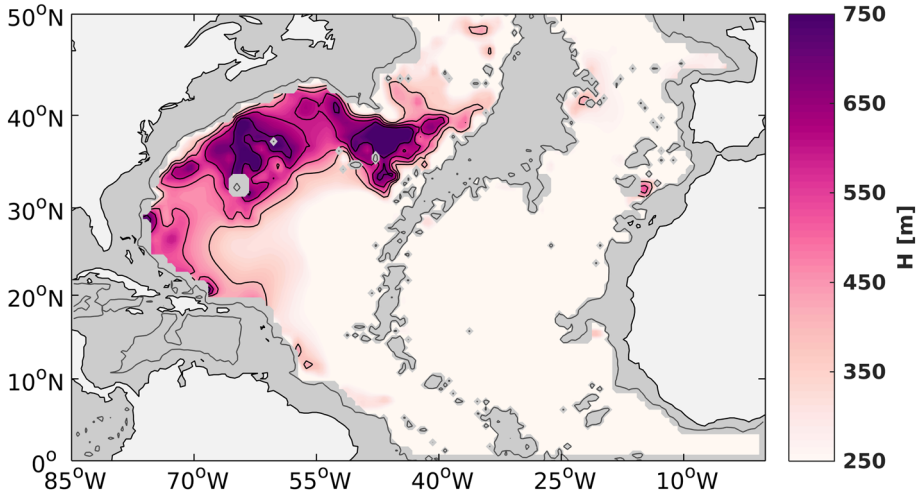

Figure 3. Maximum layer thickness, or vertical distance between σ_4 isopycnals of water with silicate below 40 µmol L^{-1}, from World Ocean Atlas 2013 data (Levitus et al., 2013). This highlights the Denmark Strait Overflow Water (DSOW), the lowest layer of NADW.

RL05.1 mascons (Save et al., 2016). Their mean differences are over 10 mm per decade, compared to 2.2 mm per decade for JPL RL05.1M, suggesting possible biases. The recently released JPL RL06 M solution is comparable to the RL05.1 M version, with an RMSD to the mooring ΔSL_{mass}(A&S) estimate of 3.6 mm per decade. A detailed analysis of the advantages and disadvantages of the different GRACE products is beyond the scope of this study, but decadal ocean mass variability in the North Atlantic seems to be represented best in the JPL mascons compared to other gridded data. The JPL RL05.1 M data are used for the remainder of this study, but the results presented here would not qualitatively change if RL06 M data were used instead.

For additional validation of GRACE ocean mass trends, ΔSL_{mass}(A&S) is also calculated using ship-based hydrography data at six locations in the Atlantic (see section 2.1). The resulting estimate of ocean mass changes is again compared to ΔSL_{mass}(G) from the GRACE JPL RL05.1 M product, shown in Figure 2 and Table 2 along with the mooring-based estimates. The hydrography data have a larger sampling error, and although they were corrected for short-term variability (Equation 4), some of the associated noise will remain in the data. Nonetheless, ΔSL_{mass} calculated from altimetry and hydrography data still agrees well with GRACE, with an RMS difference of 6.1 mm per decade. The combined RMSD between moorings and hydrography and GRACE is 5.1 mm per decade, with a correlation between ΔSL_{mass}(A&S) and ΔSL_{mass}(G) of 0.95. The mean difference is 0.4 mm per decade, suggesting that the mismatch is largely due to random variability, rather than a bias in one method relative to the other.

Thus, despite the potential additional error sources discussed in section 2.4, we find good agreement between ocean mass changes from the altimetry-steric height estimates and GRACE in the North Atlantic, supporting the veracity of GRACE trends in this region. Due to the smaller sampling error in the method, the RMSD of 3.5 mm per decade between GRACE and ocean mass calculated from mooring data is likely more indicative of the real mismatch than the RMSD between GRACE and hydrography-based ocean mass. We use this value as an estimate of the error in the GRACE trend for the remainder of this study.

3.2. Spatial Pattern of the Trend

Although ocean mass increased throughout the North Atlantic ocean, the magnitude of the trend differs between the sites studied here. A distinct spatial pattern of the trend is evident in Figure 1, with the most pronounced feature being a ridge of strong ocean mass increases extending southwestward in the interior south of the Grand Banks. The pattern resembles maps of modeled float trajectory distributions and tracers associated with Denmark Strait Overflow Water (DSOW), which comprises the lower part of NADW (Lozier, 2010; Xu et al., 2015), as well as observed distributions of hydrographic properties in this water mass. Figure 3 shows the climatological maximum layer thickness for waters with a silicate content below 40 µmol L^{-1}, which is associated with the core of DSOW. The strongest signal is found west of the Mid-Atlantic Ridge

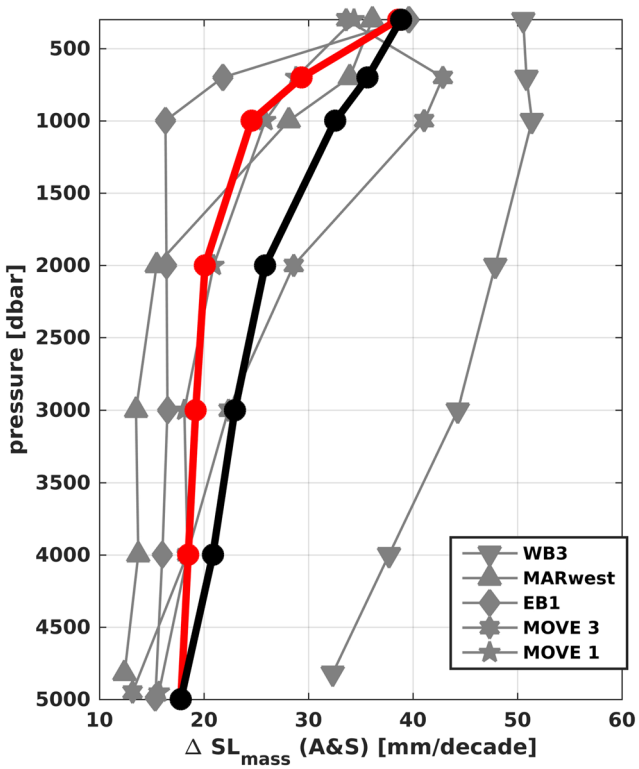

Figure 4. Ocean mass trend calculated using steric height data between the surface and each depth. The bottommost data points correspond to the full-depth estimate of ocean mass trends used in Figure 2. The thick black line shows the average of a,ll five mooring sites. The red line shows the profile that would be expected based on the global mean bias for each integration depth from Purkey et al. (2014).

(MAR) in the same interior regions where the largest trends in GRACE ocean mass occur. The resemblance between the spatial pattern of ocean mass trends and maps of NADW properties is another indication that the trend in GRACE is a real signal, as errors resulting from corrections such as those for Glacial Isostatic Adjustment (Peltier, 2009) and the pole tide (Wahr et al., 2015) have larger spatial footprints and would not be expected to align with oceanographic features. Moreover, it indicates that the decadal signal measured by GRACE is related to changes in NADW. Property distributions of NADW are a signature of its large-scale circulation (Lozier, 1997), suggesting that the changes in ocean mass observed by GRACE reflect a shift in the circulation of this water mass, which is discussed in more detail in section 4.2.

Both the comparison with an independent estimate of ocean mass changes (Figure 2 and section 3.1) and the spatial pattern of the trends (Figure 1) suggest that decadal GRACE ocean mass trends in the North Atlantic reflect real variability in the ocean. To our knowledge, this marks the first validation of decadal GRACE trends on subbasin scales. At present, the tropical/subtropical North Atlantic is the only region with a sufficient number of long-term, well-calibrated, full-depth density moorings to carry out this comparison. As a result, we cannot validate ocean mass trends in different ocean basins, but similar analyses may become possible on a global scale in the future as instrument coverage in the ocean continues to improve.

3.3. Deep Ocean Contribution to Steric Height

Many studies of the global sea level budget have used steric changes only in the upper 1,000 or 2,000 m (Cazenave et al., 2008; Ivchenko et al., 2007; Leuliette & Miller, 2009), ignoring changes below, mostly because of the better data availability in the upper ocean. Purkey et al. (2014) showed that this leads to a bias when calculating ocean mass trends as in Equation 1 of 38%, 13%, 8%, and 4% when only using data above 1,000, 2,000, 3,000, or 4,000 m for the global ocean. Figure 4 shows the ocean mass trends calculated with steric height integrated from the surface to each depth, compared to the profile using Purkey et al.'s 2014 global estimate of the bias relative to the full-depth measurement. With the exception of EB1, where the ocean below 1000 dbar barely contributes to the budget, the positive bias introduced by ignoring the deep ocean is larger at all sites compared to Purkey et al. (2014). This is particularly true for the two moorings adjacent to the western boundary, WB3 and MOVE 3, where the density of NADW has been decreasing (Frajka-Williams et al., 2018), leading to a bias of 48% and 117% in the ocean mass trend when using only steric height from 0–2,000 dbar. At the MARwest and MOVE 1 moorings, the change below 2,000 dbar is still larger than the global average, but neglecting it only leads to a bias of 25% and 33%, respectively, compared to the global average of 13%. The average trend from the five mooring sites increases by 46% (94%) when using only 0-2,000 dbar (0–1,000 dbar) steric height, much larger than the 13% (38%) in Purkey et al. (2014). This analysis shows that while measuring the deep ocean is vital for resolving the global sea level budget, its importance is also spatially variable, and these differences need to be considered in studies on more regional scales. Our data thus underline the importance of a network of sustained deep ocean density measurements from moorings, CTD transects, and the Deep Argo program (Johnson et al., 2015) for accurately monitoring long-term changes to the sea level and ocean mass budgets, particularly in the Atlantic Ocean.

4. Circulation Changes

The increase in ocean mass measured by GRACE provides information on deep ocean current changes with unprecedented spatial coverage, revealing variability along the pathways of the deep circulation. The ocean mass difference between the 2002–2009 and 2010–2017 periods in the GRACE data (Figure 1) can be used to infer horizontal gradients of OBP. These gradients are indicative of near-bottom circulation

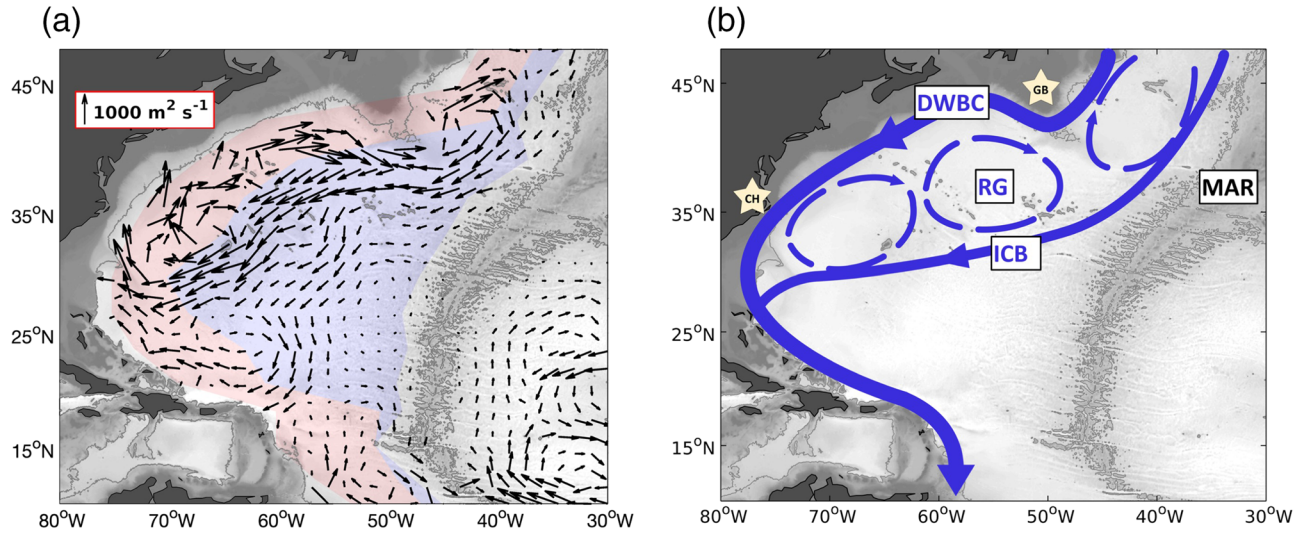

Figure 5. (left) Circulation anomalies resulting from ocean bottom pressure changes, expressed as volume transport per unit depth. Current vectors are calculated from GRACE data interpolated from the centers of the mascons to a regular grid spaced 1.5° × 1.5°. Background contours show bathymetry from Smith and Sandwell (1997). Red and blue shading highlights the boundary circulation branch and interior circulation branch, respectively, as defined in section 4.2. (right) Schematic of major features of North Atlantic Deep Water (NADW) spreading in the North Atlantic. Pathways of NADW, based on Gary et al. (2011), are shown in blue, with solid lines showing the Deep Western Boundary Current (DWBC) and interior circulation branch (ICB), and dashed lines showing the anticyclonic recirculation gyres (RG). Geographic features mentioned in the text are also marked: Grand Banks (GB), Cape Hatteras (CH), and the Mid-Atlantic Ridge (MAR).

changes (Equation 5), shown as vectors in Figure 5a. In this study, the term *circulation* is used to refer to the near-bottom velocity multiplied by the horizontal distance Δx. The decadal circulation change is dominated by a large-scale anticyclonic pattern, with northeastward flow near the coast and southwestward flow in the interior. The pattern extends from 30°N to the subpolar-subtropical gyre transition zone at about 45°N (Buckley & Marshall, 2016) and is most pronounced near the two main southward spreading paths of NADW, which are described in the following and shown schematically in Figure 5b. The most prominent pathway is the Deep Western Boundary Current (DWBC), which flows southward from the source region in the subpolar North Atlantic, following the continental slope, with a mean transport of about 20 Sv (1 Sv = 10^6 m^3 s^{-1}) (Toole et al., 2017). South of 45°N, southward flow of NADW also occurs in an interior circulation branch (ICB), which rejoins the boundary current near 30°N. Between the two branches, NADW recirculates in a clockwise, or anticyclonic, fashion in a series of eddy-driven recirculation gyres (Gary et al., 2011; Lozier, 1997). Model studies in both idealized and realistic settings (Gary et al., 2011; Lozier et al., 2013; Spall, 1996a) have suggested that the interior circulation is fed by these recirculation gyres, containing water swept away from the DWBC by eddies, which form at points where the DWBC crosses under the Gulf Stream as a result of interaction between the two currents (Spall, 1996a). The existence of an interior circulation of NADW is well established, with evidence of southward interior flow observed in hydrography (Lozier, 1997), Lagrangian float trajectories (Bower et al., 2009) and tracer distributions (Rhein et al., 2015; Smith, Smethie, et al., 2016). However, relatively little is known about either the mean transport in this branch or its variability. An overview of the North Atlantic circulation compiled from different hydrographic studies (Schmitz & McCartney, 1993) lists the interior transport as 5 Sv but relies on an assumed level of no motion for the estimate. More recent studies have largely focused on a Lagrangian assessment of particles entering the interior pathway, rather than quantitative transport estimates (Bower et al., 2009; Gary et al., 2011; Lozier, 2010; Lozier et al., 2013).

The GRACE data can help fill part of this gap in our understanding, providing information on changes in the NADW circulation, although they cannot be used to study the mean flow. In the remainder of this section, we first determine whether GRACE data can be used to study not only circulation, that is, bottom current, changes, but also changes in overall transport of NADW. This is followed by a quantitative analysis of the changes seen in Figure 5a, a discussion of the possible causes for the observed change, and an analysis of the net circulation change.

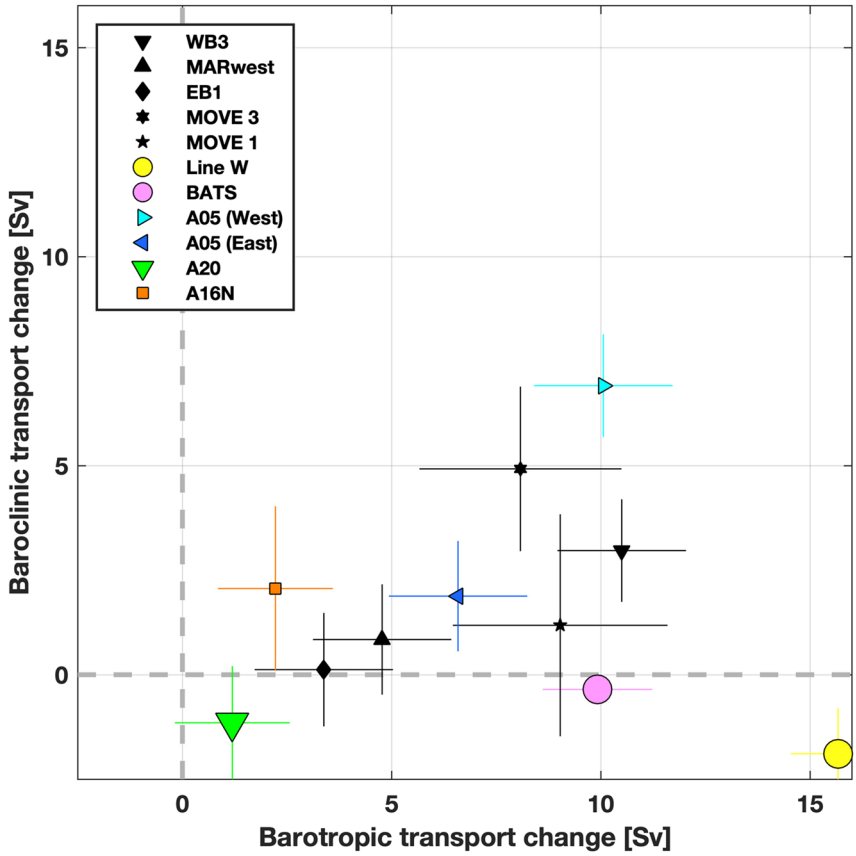

Figure 6. Barotropic transport change from GRACE compared to baroclinic transport change from density measurements, integrated between 1,000 and 4,000 dbar for each site. Periods used for the averaging are the same as in Figure 2 but are scaled to represent the change over an 8-year period, rather than a decade, to be consistent with transport changes discussed in the following section. Error bars are calculated from the steric height error in section 2.4 for the baroclinic component, and from the 3.5 mm per decade RMSD between ocean mass estimates for the barotropic component. Larger symbols highlight sites in the 30–40°N latitude range.

4.1. GRACE as a Measure of NADW Transport Change

The bottom pressure change inferred from the GRACE data can only provide information on the velocity change near the ocean bottom, and consequently the barotropic component of the transport (section 2.3). If the baroclinic (sheared) transport in the NADW layer were small, the NADW transport anomaly could then be inferred from GRACE alone by multiplying the circulation anomaly with the layer thickness which is assumed to be 3,000 m. However, this need not be the case, as the baroclinic component, which can be inferred from density gradients, can often dominate the transport variability (Send et al., 2011). Although density data are available at the sites used in this study (Figure 1), their distribution is insufficient to investigate the change in transport for the different branches of the circulation shown in Figure 5. In this section, we evaluate to what extent transport changes derived from GRACE alone are representative of the change in NADW transport and can thus be used to study the transport change without the use of colocated density measurements.

We calculate the contribution of the bottom pressure from GRACE and of density variations in the water column to the 1,000–4,000 dbar transport change of the single mooring and hydrography locations used in this study (Figure 6). This is equivalent to the barotropic and baroclinic transport change between the site in question and a point with constant OBP and density. The uncertainty for the ocean mass gradient from GRACE is estimated as 3.5 mm per decade $\times \sqrt{2} = 4.9$ mm per decade, based on the RMS difference from section 3.1. The resulting uncertainty of the change in circulation or barotropic transport is dependent on the inverse of the Coriolis parameter f, which changes with latitude. The error bars for the baroclinic change are calculated from the steric height errors discussed in section 2.4. Although the barotropic transport change

is the larger component at all sites, the baroclinic change is of similar magnitude for some locations, such as the MOVE 3 mooring and the western part of the A05 hydrography line. This suggests that using only GRACE data to infer the transport change may not be appropriate everywhere in the domain studied here. However, measurements within the latitude band from 30°N to 40°N, which features the largest circulation change observed by GRACE (Figure 5a), show a baroclinic change between −1.9 and −0.4 Sv, which is only a small part of the total transport change.

In the following section, we will investigate circulation changes throughout the domain shown in Figure 5 but discuss transport changes only for the 30–40°N range, where the change derived from GRACE alone seems to be a good approximation of the total transport. Where transport changes are discussed, we use an estimate of the error incurred by ignoring the baroclinic component of 2.9 Sv, which is calculated from World Ocean Atlas data (see Figure S2 in the supporting information).

4.2. Changes in Strength of NADW Pathways

After verifying that the decadal trends in GRACE are representative of real variability in the ocean (section 3), we now use the data to quantitatively investigate changes in NADW circulation. We focus on the region west of the MAR, where the bulk of the mean flow of NADW occurs (Lozier, 2010), and the ocean mass trends observed by GRACE are strongest (Figure 1). As discussed above, the decadal change observed by GRACE is most pronounced close to the main pathways of NADW. To quantify the circulation change between the 2002–2009 and 2010–2017 periods, we calculate at each latitude the zonally integrated change for two regions: Between the western boundary and the location of the maximum ocean mass trend from Figure 1, which marks the center of the anticyclonic circulation anomaly, and between the maximum and the MAR. We refer to the two regions as the boundary circulation branch (BCB), and interior circulation branch, ICB. The area covered for each of the regions is highlighted by the shading in Figure 5a. By construction, the sign of the change for these segments is opposite at each latitude. Due to the coarse resolution of GRACE, the Deep Western Boundary Current cannot be separated from the part of the recirculation gyre with northward mean flow (Figure 5b). As a result, changes in the BCB reflect the sum of changes to the recirculation and the DWBC. The circulation change for the two regions is shown in Figure 7 as a function of latitude.

Between 20°N and 45°N, changes for both the BCB and interior circulation are larger than the error derived in section 4.1. At every latitude in this range, the southward interior circulation branch strengthened, with opposite changes found in the boundary circulation branch. North of 30°N, the observed change is associated with the large-scale anticyclonic pattern seen in Figure 5. Changes are largest in the latitude range of 30–40°N, where the recirculation gyre and interior flow are most pronounced (Lozier, 1997, 2010). In this region, the error incurred by not having density data to resolve baroclinic changes is relatively small (section 4.1 and Figure 6), allowing us to analyze transport changes from the GRACE data alone as the circulation change multiplied by a 3,000-m layer thickness. Between 30°N and 40°N, the mean change for the interior circulation is $-4{,}638 \pm 473\ m^2\ s^{-1}$, and the associated transport change is -13.9 ± 3.3 Sv, indicative of strengthened southward advection of NADW. For the BCB, the circulation change is $3{,}561 \pm 473\ m^2\ s^{-1}$, corresponding to a change in the transport of 10.7 ± 3.3 Sv.

The 10.7 Sv change for the boundary circulation is comparable to the DWBC trend observed by current meter moorings near Line W, where transport decreased from −26.4 to −19.1 Sv between 2004 and 2014 (Toole et al., 2017). The concurrent increase in southward flow in the interior of −13.9 Sv in the present study suggests that the weaker DWBC reported by Toole et al. (2017) is not necessarily associated with an overall weakening of southward NADW transport, but rather represents an increased importance of the interior pathway relative to the DWBC. The net change from GRACE even suggests an overall strengthening of NADW circulation (black line), although the transport change is not statistically significant at -3.2 ± 3.3 Sv, and may miss some of the signal in the DWBC due to the coarse resolution of the data. In a Lagrangian model study of NADW pathways, Bower et al. (2009) showed that most NADW water parcels are found in the interior as opposed to the DWBC between 42°N and 30°N and suggested that the interior branch may be the main pathway for NADW in this latitude range. The strengthening of the interior circulation branch by −13.9 Sv shown here, more than half the mean strength of the DWBC, suggests that pathways in the interior have become even more important since Bower et al.'s (2009) study.

The NADW transport and circulation changes discussed above and shown in Figures 5 and 7 add to the growing evidence that interior pathways play a significant role in the spreading of NADW from its formation

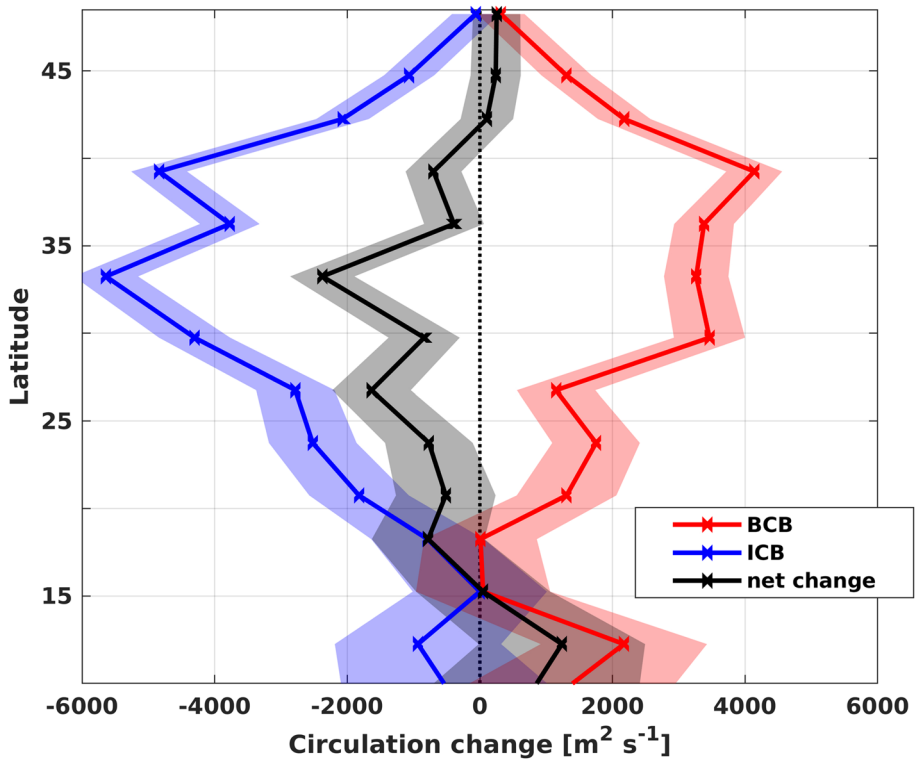

Figure 7. The 1 April 2010 to 31 March 2017 minus 1 April 2002 to 31 March 2009 circulation change from GRACE, calculated for two regions (see text and Figure 5a for definitions). Red: boundary circulation branch. Blue: interior circulation branch. Black: Sum of the two. Shading represents uncertainty in the circulation change, which increases toward the equator as f becomes smaller.

region (Bower et al., 2009, 2019; Getzlaff et al., 2006; Lozier, 2010). While those previous studies focused mostly on the mean state, our results show that the importance of these different branches can also change substantially over time, highlighting the need for an improved understanding of the underlying dynamics.

4.3. Possible Causes of Variability

The changes discussed above may represent either a longer-term shift toward increased NADW flow in the interior, or part of a cycle of natural variability on multidecadal time scales. In this section, we summarize several modes of multidecadal variability in the Atlantic ocean, and discuss how the strengthened interior circulation observed by GRACE could be related to each of them. The Deep Western Boundary Current, Gulf Stream, and interior pathways are linked dynamically through their interactions at the crossover points such as the Grand Banks near 42°N (Bower et al., 2009; Gary et al., 2011) and Cape Hatteras near 35°N, where deep eddies entrain water from the DWBC into the recirculation gyres (Spall, 1996a). Due to this interaction with the surface circulation, Lozier (2010) proposed that the strength of the ICB could be affected by atmospheric forcing. The major mode of interannual to multidecadal atmospheric variability over the Atlantic Ocean is the North Atlantic Oscillation, or NAO. The positive phase of the NAO is associated with an increase in atmospherically driven variability in the ocean, such as a stronger Gulf Stream and North Atlantic Current (Curry & McCartney, 2001). During the 2010–2017 period, the NAO was predominantly in its positive phase. Increased surface circulation in the subtropical gyre (Thompson et al., 2018) and reduced renewal of Eighteen Degree Water in the surface layer of the recirculation gyre (Billheimer & Talley, 2013, 2016) have both been linked to this persistent positive phase of the NAO. The increase in interior flow reported here could likewise be related to the prolonged period of positive NAO, with changes in surface forcing communicated to the deep ocean at the crossover points as proposed by Lozier (2010). In addition to the decadal change discussed throughout this study, the strength of the ICB measured by GRACE also varies over an annual cycle, with a peak-to-peak amplitude of 7 Sv from April to October (Figure 8), and an opposing seasonal cycle for the BCB. This seasonal dependence of the transport supports a connection to surface processes, although the forcing controlling seasonal and decadal variability may not necessarily be the same.

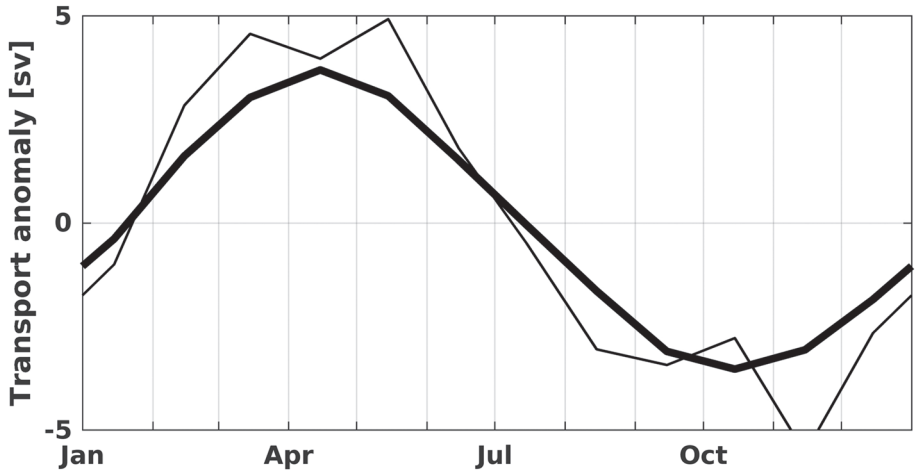

Figure 8. Annual cycle of barotropic transport in the interior circulation branch from GRACE data. Thin line shows monthly means; thick line is a five-point running mean.

The circulation of NADW has been linked to the highly variable formation of Labrador Sea Water (LSW), one of the main water masses making up NADW, in the source region (Yashayaev & Loder, 2016). Although recent results have called into question the effect of LSW formation rate on net transport (Lozier et al., 2019), other aspects of the circulation could still be affected. The increase in interior transport shown here coincides with deeper convection starting in 2012, and extending to depths close to the record values of the mid-1990s in 2016 (Yashayaev & Loder, 2017), after relatively weak LSW formation in the previous decade. Yashayaev and Loder (2016) showed that the export of LSW from the Labrador Sea is larger in years with deeper convection, and such an increase in LSW export after 2012 could be related to the strengthened interior circulation observed in the present study. However, LSW formation is also strongly affected by the NAO, so the simultaneous increase in interior flow of NADW and convection depth in the Labrador Sea may simply be a result of the effect of atmospheric forcing on both.

Another possible explanation is internal variability of the recirculation gyre leading to stronger interior transport, as found in an idealized model by Spall (1996b). In the model, the feedback between Gulf Stream instabilities, eddies carrying water from the DWBC into the recirculation gyre, and recirculation strength causes oscillations in the system on multidecadal time scales. Andres (2016) reported a decrease in Gulf Stream stability after 2008 and an associated increase in deep eddy activity and proposed that these changes could be related to such internal variability. A subsequent increase in interior NADW transport would be consistent with variability in this internal mode, representing a shift from the low energy to the high energy state. In the model, increasing transport in the interior circulation branch is entirely fed by a larger fraction of NADW diverted away from the DWBC with no net transport change, which would lead to a weakened DWBC as observed by Toole et al. (2017). While the observed changes are similar to those proposed for this mode of variability, the oscillations in the simple three-layer model by Spall (1996b) affect mostly the upper core of the DWBC. In contrast, the interior transport change reported here is largely barotropic within the NADW layer, affecting both upper and lower North Atlantic Deep Water. More realistic models will be needed to determine whether variability associated with these internal oscillations can also extend to the lower part of NADW.

Regardless of the underlying causes, the observed change in the partitioning between the different pathways has important implications for measuring the AMOC: In tracer studies, for a given amount of net NADW transport, a weakened DWBC with a compensating increase in transport in the interior would increase the mean transit time, and could be erroneously attributed to a weakened overall southward flow of NADW (Lozier, 2010). In addition, a major motivation for studying the deep circulation is the spreading of dissolved gases such as carbon dioxide (Sabine et al., 2004), which will be affected by variability in the relative importance of boundary and interior routes (Rhein et al., 2015). If the changes seen here represent a shift toward a strengthened interior circulation, the properties of deep water throughout the Atlantic will be profoundly affected. If the changes are related to natural variability on decadal or multidecadal time scales, such as that associated with the mechanisms discussed above, a decrease in the strength of the ICB would be expected

to follow in the near future. Additional measurements over the next decades, such as from the GRACE Follow-On mission, as well as dedicated model studies, will be necessary to better understand the causes for the observed change in the strength of the different NADW pathways.

4.4. Net Circulation Change West of the MAR

Although most of the variability described above is associated with compensating northward and southward flow, there is also a *net* change in bottom circulation in the western North Atlantic. Unlike the net transport change discussed in section 4.2, the net circulation change in much of the basin is different from 0 within the uncertainty as defined in section 4.1. Everywhere between 18°N and 40°N, the net circulation change is negative, with a mean change in this latitude range of $-1{,}000 \pm 593\,m^2\,s^{-1}$ (Figure 7, black line). This means that zonally integrated deep velocities in the western subtropical Atlantic have generally become more southward from the 2002–2009 to the 2010–2017 period.

At 15°N, the net circulation change is close to zero at $48 \pm 1{,}011\,m^2\,s^{-1}$, supporting the assumption made in the nearby MOVE array that the flow at the reference level is negligible on long time scales at this latitude (Send et al., 2011). At 27°N, the 8-year bottom circulation change is $-1{,}633 \pm 591\,m^2\,s^{-1}$, opposite to the trend reported for the RAPID array at 26.5°N, where the constraint of mass conservation yields a northward trend in the reference level flow of about 10^{-4} Sv m^{-1} $year^{-1}$, or $1{,}000\,m^2\,s^{-1}$ per decade, from 2004 to 2014 (Frajka-Williams et al., 2016). The deep changes inferred from GRACE remain southward if the analysis is extended across the entire width of the Atlantic to mimic the coverage of the RAPID array. The disagreement between GRACE and RAPID trends has been noted previously and attributed to possible errors in the decadal variability in GRACE data (Worthington et al., 2019). To account for the difference between trends in RAPID and the GRACE JPL RL05.1 M product, the error in the decadal trends of the zonal ocean mass gradient would have to be 23.3 mm per decade. In the present study, the GRACE-derived gradient between WB3 and MARwest differs from independent (altimetry and mooring) ocean mass measurements by only 3 mm per decade (Table 2). It therefore seems unlikely that GRACE errors alone can be responsible for the disagreement between the deep RAPID and GRACE trends. Some of the difference may be explained by the RAPID compensation term, T_{ext} (McCarthy et al., 2015), not strictly corresponding to a reference level velocity. For example, a change occurring in regions not sampled by the array, such as the "bottom triangles" between moorings near the boundaries and MAR, would also be included in the compensation term. The discrepancy between GRACE and the external transport in RAPID will be explored further in a future study, which uses GRACE along with mooring density data from MOVE and RAPID to resolve the variability of both the barotropic and baroclinic component of NADW transport at 16°N and 26.5°N.

5. Summary

In this study, trends in the GRACE JPL RL05.1 M product (Watkins et al., 2015) were validated against ocean mass calculated from altimetry and moorings at five sites, showing consistent increases in ocean mass in the subtropical and tropical North Atlantic ocean (Figure 2). The mean trends are 17.8 ± 5.2 mm per decade for the altimetry-mooring estimate, and 15.6 ± 1.8 mm per decade from GRACE. The RMS difference between the methods is 3.5 mm per decade, suggesting that the long-term changes seen in GRACE data reflect real changes in the ocean. GRACE trends are also compared against a more uncertain estimate using hydrography instead of mooring data, again showing consistent trends, with an RMSD of 6.1 mm per decade. The GRACE ocean mass trends are further supported by a close resemblance of their spatial pattern to property distributions in the NADW layer. Changes in the deep ocean below 2,000 dbar play an important part in the ocean mass budget, especially near the western boundary, showing the importance of resolving the full water column in studies of global sea level. The present study focuses on the North Atlantic, which is the region with the highest number of sustained long-term ocean monitoring efforts that can be used to verify trends in GRACE ocean mass. Deploying thoroughly calibrated moorings in other parts of the world ocean would be beneficial for validating ocean mass and altimetry measurements from future satellite missions on a global scale.

Ocean mass changes between the 2002–2009 and 2010–2017 periods indicate changes in the circulation of North Atlantic Deep Water in the western North Atlantic (Figure 5): For the boundary circulation branch, the transport changes by 10.7 ± 3.3 Sv between 30°N and 40°. The change represents a weakening of the time-mean southward transport, and is comparable to trends observed by Toole et al. (2017) for the Deep

Western Boundary Current. This is balanced by a strengthened interior circulation branch of NADW, with southward transport increasing by -13.9 ± 3.3 Sv. The net bottom circulation change between 18°N and 40°N west of the MAR is $-1,000 \pm 593\ m^2\ s^{-1}$, reflecting an overall increase of southward flow at depth, but net transport changes are not significant. At 15°N, the net circulation change is only $48 \pm 1,011\ m^2\ s^{-1}$, consistent with the assumption made in Send et al. (2011) that long-term changes in the near-bottom flow are negligible at this latitude. At 27°N, the circulation change is $-1,633 \pm 591\ m^2\ s^{-1}$, which is of opposing sign compared to the external transport from the nearby RAPID array (McCarthy et al., 2015). A number of earlier studies had attributed this discrepancy to errors in the geophysical corrections of GRACE, but our results suggest that these errors are smaller than previously thought.

Possible causes for the observed changes in the deep circulation of the Atlantic ocean include variability in surface atmospheric forcing as part of the NAO, variable rates of deep water formation, or internal variability. The decadal changes measured by GRACE imply a major increase in the relative importance of interior flow compared to advection in the DWBC for the southward spreading of NADW between the 2000s and the 2010s. This supports the view that interior pathways play a fundamental role in the equatorward transport of NADW (Lozier, 2010), as opposed to the classical picture of a deep circulation dominated by the DWBC (Stommel & Arons, 1959). Our results show that the interior circulation is not only important for the distribution of NADW in the mean state, but also varies in strength on decadal time scales, highlighting the need for sustained observations of both the boundary and interior regions for fully resolving the variability of the deep circulation.

Data Availability Statement

MOVE data are freely available through OceanSITES. GRACE ocean data are available online (http://grace.jpl.nasa.gov), supported by the NASA MEaSUREs Program. Data sources for all data used in this study are listed in Table 1.

Acknowledgments
J. K. was supported by NASA Headquarters under the NASA Earth and Space Science Fellowship Program (Grant NNX16AO39H). MOVE is presently supported by NOAA GOMO under award NA20OAR4320278. MOVE was previously supported by the German BMBF. Data from the RAPID-WATCH MOC monitoring project are funded by NERC (UK) and are freely available online (http://www.rapid.ac.uk/rapidmoc). The Ssalto/Duacs altimeter products were produced and distributed by the Copernicus Marine and Environment Monitoring Service (CMEMS) (http://www.marine.copernicus.eu). The authors would like to thank Eleanor Frajka-Williams and Felix Landerer for helpful discussions and comments. We would also like to thank two anonymous reviewers, whose comments helped improve the manuscript.

References

Ablain, M., Cazenave, A., Larnicol, G., Balmaseda, M., Cipollini, P., Faugère, Y., et al. (2015). Improved sea level record over the satellite altimetry era (1993–2010) from the Climate Change Initiative project. *Ocean Science*, *11*(1), 67–82. https://doi.org/10.5194/os-11-67-2015

Andres, M. (2016). On the recent destabilization of the Gulf Stream path downstream of Cape Hatteras. *Geophysical Research Letters*, *43*, 9836–9842. https://doi.org/10.1002/2016GL069966

Billheimer, S., & Talley, L. D. (2013). Near cessation of eighteen degree water renewal in the Western North Atlantic in the warm winter of 2011–2012. *Journal of Geophysical Research: Oceans*, *118*, 6838–6853. https://doi.org/10.1002/2013JC009024

Billheimer, S., & Talley, L. D. (2016). Extraordinarily weak Eighteen Degree Water production concurs with strongly positive North Atlantic Oscillation in late winter 2014/15. In *State of the climate in 2015* (Vol. 97, pp. S78–S79).

Bower, A. S., Lozier, S., Biastoch, A., Drouin, K., Foukal, N., Furey, H., et al. (2019). Lagrangian views of the pathways of the atlantic meridional overturning circulation. *Journal of Geophysical Research: Oceans*, *124*, 5313–5335. https://doi.org/10.1029/2019JC015014

Bower, A. S., Lozier, M. S., Gary, S. F., & Böning, C. W. (2009). Interior pathways of the North Atlantic meridional overturning circulation. *Nature*, *459*(7244), 243. https://doi.org/10.1038/nature07979

Buckley, M. W., & Marshall, J. (2016). Observations, inferences, and mechanisms of the Atlantic Meridional Overturning Circulation: A review. *Reviews of Geophysics*, *54*, 5–63. https://doi.org/10.1002/2015RG000493

Cazenave, A., Dominh, K., Guinehut, S., Berthier, E., Llovel, W., Ramillien, G., et al. (2008). Sea level budget over 2003–2008: A reevaluation from GRACE space gravimetry, satellite altimetry and Argo. *Global and Planetary Change*, *65*(1–2), 83–88. https://doi.org/10.1016/j.gloplacha.2008.10.004

Chambers, D. P., Cazenave, A., Champollion, N., Dieng, H., Llovel, W., Forsberg, R., et al. (2017). Evaluation of the Global Mean Sea Level Budget between 1993 and 2014. *Integrative study of the mean sea level and its components* (Vol. 38, pp. 315–333). Cham: Springer. https://doi.org/10.1007/s10712-016-9381-3

Chelton, D. B., Ries, J. C., Haines, B. J., & Callahan, P. S. (2001). Chapter 1 satellite altimetry. *International Geophysics*, *69*, 1–ii. https://doi.org/10.1016/S0074-6142(01)80146-7

Curry, R. G., & McCartney, M. S. (2001). Ocean gyre circulation changes associated with the North Atlantic Oscillation. *Journal of Physical Oceanography*, *31*(12), 3374–3400. https://doi.org/10.1175/1520-0485(2001)031<3374:OGCCAW>2.0.CO;2

Danabasoglu, G. (2008). On multidecadal variability of the Atlantic Meridional Overturning Circulation in the Community Climate System Model version 3. *Journal of Climate*, *21*(21), 5524–5544. https://doi.org/10.1175/2008JCLI2019.1

Frajka-Williams, E., Lankhorst, M., Koelling, J., & Send, U. (2018). Coherent circulation changes in the deep North Atlantic from 16°N and 26°N transport arrays. *Journal of Geophysical Research: Oceans*, *123*, 3427–3443. https://doi.org/10.1029/2018JC013949

Frajka-Williams, E., Meinen, C. S., Johns, W. E., Smeed, D. A., Duchez, A., Lawrence, A. J., et al. (2016). Compensation between meridional flow components of the Atlantic MOC at 26°N. *Ocean Science*, *12*(2), 481–493. https://doi.org/10.5194/os-12-481-2016

Gary, S. F., Susan Lozier, M., Böning, C. W., & Biastoch, A. (2011). Deciphering the pathways for the deep limb of the Meridional Overturning Circulation. *Deep Sea Research Part II: Topical Studies in Oceanography*, *58*(17–18), 1781–1797. https://doi.org/10.1016/J.DSR2.2010.10.059

Getzlaff, K., Böning, C. W., & Dengg, J. (2006). Lagrangian perspectives of deep water export from the subpolar North Atlantic. *Geophysical Research Letters*, *33*, L21S08. https://doi.org/10.1029/2006GL026470

Guo, J. Y., Duan, X. J., & Shum, C. K. (2010). Non-isotropic Gaussian smoothing and leakage reduction for determining mass changes over land and ocean using GRACE data. *Geophysical Journal International*, *181*(1), 290–302. https://doi.org/10.1111/j.1365-246X.2010.04534.x

Houston, M. H., & Paros, J. M. (1998). High accuracy pressure instrumentation for underwater applications. In *Ut 1998 - proceedings of the 1998 international symposium on underwater technology* (pp. 307–311). IEEE.

IOCCP-ICPO (2010). The GO-SHIP repeat hydrography manual: A collection of expert reports and guidelines. IOCCP Report Number 14, ICPO Publication Series Number 134. IOCCP Rep, 14.

Ivchenko, V. O., Danilov, S. D., Sidorenko, D. V., Schröter, J., Wenzel, M., & Aleynik, D. L. (2007). Comparing the steric height in the Northern Atlantic with satellite altimetry. *Ocean Science*, *3*(4), 485–490. https://doi.org/10.5194/os-3-485-2007

Johnson, G. C., Lyman, J. M., & Purkey, S. G. (2015). Informing deep argo array design using argo and full-depth hydrographic section data. *Journal of Atmospheric and Oceanic Technology*, *32*(11), 2187–2198. https://doi.org/10.1175/JTECH-D-15-0139.1

Kanzow, T., Send, U., Zenk, W., Chave, A. D., & Rhein, M. (2006). Monitoring the integrated deep meridional flow in the tropical North Atlantic: Long-term performance of a geostrophic array. *Deep-Sea Research Part I: Oceanographic Research Papers*, *53*(3), 528–546. https://doi.org/10.1016/j.dsr.2005.12.007

Landerer, F. W., Flechtner, F. M., Save, H., Webb, F. H., Bandikova, T., Bertiger, W. I., et al. (2020). Extending the global mass change data record: GRACE follow-on instrument and science data performance. *Geophysical Research Letters*, *47*, e2020GL088306. https://doi.org/10.1029/2020GL088306

Landerer, F. W., Wiese, D. N., Bentel, K., Boening, C., & Watkins, M. M. (2015). North Atlantic meridional overturning circulation variations from GRACE ocean bottom pressure anomalies. *Geophysical Research Letters*, *42*, 8114–8121. https://doi.org/10.1002/2015GL065730

Leith, C. E. (1973). The standard error of time-average estimates of climatic means. *Journal of Applied Meteorology*, *12*(6), 1066–1069. https://doi.org/10.1175/1520-0450(1973)012<1066:tseota>2.0.co;2

Leuliette, E. W., & Miller, L. (2009). Closing the sea level rise budget with altimetry, Argo, and Grace. *Geophysical Research Letters*, *36*, L04608. https://doi.org/10.1029/2008GL036010

Levitus, S., Antonov, J. I., Baranova, O. K., Boyer, T. P., Coleman, C. L., Garcia, H. E., et al. (2013). The world ocean database. *Data Science Journal*, *12*, WDS229–WDS234. https://doi.org/10.2481/dsj.WDS-041

Lozier, M. S. (1997). Evidence for large-scale eddy-driven gyres in the North Atlantic. *Science*, *277*(5324), 361–364. https://doi.org/10.1126/science.277.5324.361

Lozier, M. S. (2010). Deconstructing the conveyor belt. *Science*, *328*(5985), 1507–1511. https://doi.org/10.1126/science.1189250

Lozier, M. S., Gary, S. F., & Bower, A. S. (2013). Simulated pathways of the overflow waters in the North Atlantic: Subpolar to subtropical export. *Deep Sea Research Part II: Topical Studies in Oceanography*, *85*, 147–153. https://doi.org/10.1016/J.DSR2.2012.07.037

Lozier, M. S., Li, F., Bacon, S., Bahr, F., Bower, A. S., Cunningham, S. A., et al. (2019). A sea change in our view of overturning in the subpolar North Atlantic. *Science*, *363*(6426), 516–521. https://doi.org/10.1126/science.aau6592

Mazloff, M. R., & Boening, C. (2016). Rapid variability of Antarctic Bottom Water transport into the Pacific Ocean inferred from GRACE. *Geophysical Research Letters*, *43*, 3822–3829. https://doi.org/10.1002/2016GL068474

McCarthy, G. D., Smeed, D. A., Johns, W. E., Frajka-Williams, E., Moat, B. I., Rayner, D., et al. (2015). Measuring the Atlantic Meridional Overturning Circulation at 26 °N. *Progress in Oceanography*, *130*, 91–111. https://doi.org/10.1016/J.POCEAN.2014.10.006

Muir, L. C., & Fedorov, A. V. (2017). Evidence of the AMOC interdecadal mode related to westward propagation of temperature anomalies in CMIP5 models. *Climate Dynamics*, *48*(5–6), 1517–1535. https://doi.org/10.1007/s00382-016-3157-9

Peltier, W. R. (2009). Closure of the budget of global sea level rise over the GRACE era: the importance and magnitudes of the required corrections for global glacial isostatic adjustment. *Quaternary Science Reviews*, *28*(17), 1658–1674. https://doi.org/10.1016/j.quascirev.2009.04.004

Purkey, S. G., Johnson, G. C., & Chambers, D. P. (2014). Relative contributions of ocean mass and deep steric changes to sea level rise between 1993 and 2013. *Journal of Geophysical Research: Oceans*, *119*, 7509–7522. https://doi.org/10.1002/2014JC010180

Quinn, K. J., & Ponte, R. M. (2010). Uncertainty in ocean mass trends from GRACE. *Geophysical Journal International*, *181*(2), 762–768. https://doi.org/10.1111/j.1365-246X.2010.04508.x

Rhein, M., Kieke, D., & Steinfeldt, R. (2015). Advection of North Atlantic Deep Water from the Labrador Sea to the southern hemisphere. *Journal of Geophysical Research: Oceans*, *120*, 2471–2487. https://doi.org/10.1002/2014JC010605

Sabine, C. L., Feely, R. A., Gruber, N., Key, R. M., Lee, K., Bullister, J. L., et al. (2004). The oceanic sink for anthropogenic CO_2. *Science*, *305*(5682), 367–371.

Save, H., Bettadpur, S., & Tapley, B. D. (2016). High-resolution CSR GRACE RL05 mascons. *Journal of Geophysical Research: Solid Earth*, *121*, 7547–7569. https://doi.org/10.1002/2016JB013007

Schmitz, W. J., & McCartney, M. S. (1993). On the North Atlantic Circulation. *Reviews of Geophysics*, *31*(1), 29–49. https://doi.org/10.1029/92RG02583

Send, U., Lankhorst, M., & Kanzow, T. (2011). Observation of decadal change in the Atlantic meridional overturning circulation using 10 years of continuous transport data. *Geophysical Research Letters*, *38*, L24606. https://doi.org/10.1029/2011GL049801

Smeed, D. A., McCarthy, G. D., Cunningham, S. A., Frajka-Williams, E., Rayner, D., Johns, W. E., et al. (2014). Observed decline of the Atlantic meridional overturning circulation 2004–2012. *Ocean Science*, *10*(1), 29–38. https://doi.org/10.5194/os-10-29-2014

Smeed, D. A., Moat, B., Rayner, D., Johns, W. E., Baringer, M. O., Volkov, D., & Frajka-Williams, E. (2019). Atlantic meridional overturning circulation observed by the RAPID-MOCHA-WBTS (RAPID-Meridional overturning circulation and heatflux array-Western boundary time series) array at 26N from 2004 to 2018. British Oceanographic Data Centre - Natural Environment Research Council, UK.

Smith, W. H. F., & Sandwell, D. T. (1997). Global sea floor topography from satellite altimetry and ship depth soundings. *Science*, *277*(5334), 1956–1962. https://doi.org/10.1126/science.277.5334.1956

Smith, J. N., Smethie, W. M., Yashayev, I., Curry, R., & Azetsu-Scott, K. (2016). Time series measurements of transient tracers and tracer-derived transport in the Deep Western Boundary Current between the Labrador Sea and the subtropical Atlantic Ocean at Line W. *Journal of Geophysical Research: Oceans*, *121*, 8115–8138. https://doi.org/10.1002/2016JC011759

Spall, M. A. (1996a). Dynamics of the gulf stream/deep western boundary current crossover. Part I: Entrainment and recirculation. *Journal of Physical Oceanography*, *26*(10), 2152–2168. https://doi.org/10.1175/1520-0485(1996)026<2152:DOTGSW>2.0.CO;2

Spall, M. A. (1996b). Dynamics of the gulf stream/deep western boundary current crossover. Part II: Low-frequency internal oscillations. *Journal of Physical Oceanography*, *26*(10), 2169–2182. https://doi.org/10.1175/1520-0485(1996)026<2169:DOTGSW>2.0.CO;2

Srokosz, M. A., & Bryden, H. L. (2015). Observing the Atlantic Meridional Overturning Circulation yields a decade of inevitable surprises. *Science*, *348*(6241), 1,255,575–1,255,575. https://doi.org/10.1126/science.1255575

Stommel, H., & Arons, A. B. (1959). On the abyssal circulation of the world ocean—I. Stationary planetary flow patterns on a sphere. *Deep Sea Research (1953)*, *6*(C), 140–154. https://doi.org/10.1016/0146-6313(59)90065-6

Talley, L. D., Pickard, G. L., Emery, W. J., & Swift, J. H. (2012). Dynamical processes for descriptive ocean circulation. Descriptive Physical Oceanography, 187–221, https://doi.org/10.1016/b978-0-7506-4552-2.10007-1

Tapley, B. D., Bettadpur, S., Watkins, M., & Reigber, C. (2004). The gravity recovery and climate experiment: Mission overview and early results. *Geophysical Research Letters*, *31*, L09607. https://doi.org/10.1029/2004GL019920

Thompson, P. R., Merrifield, M. A., Leuliette, E., Sweet, W., Chambers, D. P., Hamlington, B. D., et al. (2018). Sea level variability and change. *State of the climate in 2017* (Vol. 99, pp. S84–S86).

Toole, J. M., Andres, M., Le Bras, I. A., Joyce, T. M., & McCartney, M. S. (2017). Moored observations of the Deep Western Boundary Current in the NW Atlantic: 2004–2014. *Journal of Geophysical Research: Oceans*, *122*, 7488–7505. https://doi.org/10.1002/2017JC012984

Wahr, J., Nerem, R. S., & Bettadpur, S. V. (2015). The pole tide and its effect on GRACE time-variable gravity measurements: Implications for estimates of surface mass variations. *Journal of Geophysical Research: Solid Earth*, *120*, 4597–4615. https://doi.org/10.1002/2015JB011986

Watkins, M. M., Wiese, D. N., Yuan, D.-N., Boening, C., & Landerer, F. W. (2015). Improved methods for observing Earth's time variable mass distribution with GRACE using spherical cap mascons. *Journal of Geophysical Research: Solid Earth*, *120*, 2648–2671. https://doi.org/10.1002/2014JB011547

Watts, D. R., & Kontoyiannis, H. (1990). Deep-ocean bottom pressure measurement: Drift removal and performance. *Journal of Atmospheric and Oceanic Technology*, *7*(2), 296–306. https://doi.org/10.1175/1520-0426(1990)007<0296:dobpmd>2.0.co;2

Wiese, D. N., Landerer, F. W., & Watkins, M. M. (2016). Quantifying and reducing leakage errors in the JPL RL05M GRACE mascon solution. *Water Resources Research*, *52*, 7490–7502. https://doi.org/10.1002/2016WR019344

Williams, J., Hughes, C. W., & Tamisiea, M. E. (2015). Detecting trends in bottom pressure measured using a tall mooring and altimetry. *Journal of Geophysical Research: Oceans*, *120*, 5216–5232. https://doi.org/10.1002/2015JC010955

Worthington, E. L., Frajka-Williams, E., & McCarthy, G. D. (2019). Estimating the deep overturning transport variability at 26°N using bottom pressure recorders. *Journal of Geophysical Research: Oceans*, *124*, 335–348. https://doi.org/10.1029/2018JC014221

Xu, X., Rhines, P. B., Chassignet, E. P., & Schmitz, W. J. (2015). Spreading of Denmark strait overflow water in the Western Subpolar North Atlantic: Insights from eddy-resolving simulations with a passive tracer. *Journal of Physical Oceanography*, *45*(12), 2913–2932.

Yashayaev, I., & Loder, J. W. (2016). Recurrent replenishment of Labrador Sea Water and associated decadal-scale variability. *Journal of Geophysical Research: Oceans*, *121*, 8095–8114. https://doi.org/10.1002/2016JC012046

Yashayaev, I., & Loder, J. W. (2017). Further intensification of deep convection in the labrador sea in 2016. *Geophysical Research Letters*, *44*, 1429–1438. https://doi.org/10.1002/2016GL071668